Journal of ELECTRONIC MATERIALS, Vol. 47, No. 12, 2018
https://doi.org/10.1007/s11664-018-6673-z
© 2018 The Minerals, Metals & Materials Society

Light-Enhanced Vanadium Pentoxide (V_2O_5) Thin Films for Gas Sensor Applications

TARIQ ABDUL-HAMEED ABBAS[1,2]

1.—Physics Department, College of Science, Salahaddin University, Erbil, Kurdistan, Iraq. 2.—e-mail: dr_t_abbas@yahoo.com

Generally, semiconductors such as SnO_2, ZnO, and Fe_2O_3 are mostly used for gas detection. However, low sensitivity and high operating temperature limit their optoelectronic application, hence the need for viable alternative semiconductors. Vanadium pentoxide (V_2O_5) was selected for this study because of its layered structure and different valence states. V_2O_5 nanostructures were deposited on preheated glass substrates using the spray pyrolysis technique. Structural and morphological properties of the V_2O_5 nanoparticles were studied using x-ray diffraction (XRD) analysis and field-emission scanning electron microscopy (FESEM). The results reveal an orthorhombic structure with preferred orientation along (001) plane and average grain size of 27.179 nm. A $V_2O_5/SiO_2/Si$ gas sensor device was fabricated by depositing the V_2O_5 nanostructures on oxidized *p*-type silicon substrate. The current–voltage (*I*–*V*) characteristic and response of the sensor to different concentrations of ethanol and acetone gases at different operating temperatures were investigated. The light-enhanced sensor response was also studied under illumination from a green laser source. The sensing mechanism for the V_2O_5 nanostructures with and without illumination was also determined. The sensitivity of the $V_2O_5/SiO_2/Si$ gas sensor to ethanol and acetone was higher at low operating temperatures (40°C to 50°C). The gas sensor was more sensitive to ethanol than acetone at room temperature under both dark and illumination conditions. The results also indicated higher sensitivity under light illumination compared with dark conditions. In addition, the fabricated sensor exhibited faster response/recovery time for ethanol (43.493 μs/195.42 μs) than acetone (43.2001 μs/214.17 μs) at exposure duration of 10 min. Therefore, the application of V_2O_5 nanostructures is promising for detection of both acetone and (particularly) ethanol at low operating temperatures.

Key words: Vanadium pentoxide nanostructures, gas sensor, sensitivity, light illumination, ethanol, acetone

INTRODUCTION

Extensive research is currently being conducted to develop high-gain and low-noise optical devices. The physical and chemical properties of semiconducting thin-film materials differ from their bulk counterparts. Therefore, preparation techniques and deposition processes used to create thin films (nanostructures) can change their physical properties, subsequently affecting their potential applications. This has now been recognized internationally, and novel materials with unique intrinsic properties are being developed.[1–5]

A gas sensor detects various gases in different atmospheres, transforming the chemical reactions to analytically useful detectable signals.[6,7] A sensor may provide different types of output, but typically produces electrical or optical signals. The efficiency of a gas sensor depends on the kind of gas, its

(Received April 21, 2018; accepted September 11, 2018; published online September 25, 2018)

concentration, the materials of the sensor, and the output due to the interaction of the gas with the material on the surface of the sensor.[1,7] Temperature is an important factor that controls such interaction of gas with materials on the surface of the sensor.[8,9] Each gas has an optimum temperature for this interaction.[10] The operating temperature also determines the response of thin films in the gas sensing mechanism.[11–13] Thus, increasing the operation temperature enhances the sensitivity of the films. However, gas at room temperature has no effect on the film conductivity, even with increase in its concentration. Therefore, reducing the operating temperature of gas sensors while maintaining their stability and sensitivity is important.[14–17] Light illumination is one of the methods used to improve gas sensitivity at low operating temperatures. Recently, there have been reports of gas sensors based on photoactivation of metal-oxide semiconductors.[18–20] Moreover, light Illumination of gas sensors has been shown to be a feasible alternative for activation of chemical reactions on the surface of oxides without heating.[21–23]

Transition-metal oxides can sense gases by changing their electrical conductance reversibly when the composition of the surrounding atmosphere is altered, i.e., gas detection based on the interaction between the surface of the sensing element and the surrounding gaseous atmosphere.[14] Semiconductors such as SnO_2, ZnO, and Fe_2O_3 are mostly used for such detection of ethanol gas. However, low sensitivity and high operating temperature limit their application, hence the need to explore new and viable alternative materials. Therefore, vanadium pentoxide (V_2O_5) has been suggested for various optoelectronic applications,[2,3] particularly as a gas sensor, because of its exceptional intrinsic properties.[1,4,5] One-dimensional-structured V_2O_5 has a promising future for production of gas sensors that could be operated at room temperature.[6] As a transition-metal-oxide semiconductor, V_2O_5 has attracted considerable interest over the years due to its unique layered structure, various valence states,[6] and wide range of applications.[3,15,16] V_2O_5 is an *n*-type semiconductor that is both stable and has high oxidation state.[10,17] Furthermore, V_2O_5 contains active sites for adsorption of gaseous molecules on the surface.[11] It has many interesting features, such as layered structure, wide optical bandgap (2.44 eV), multivalency, and good chemical and thermal stability. Due to these properties, vanadium pentoxide is a potential candidate for gas sensing.[11,16]

V_2O_5 thin films can be obtained using different techniques such as thermal evaporation, the sol–gel process, magnetron sputtering, chemical vapor deposition, electron beam evaporation, and spray pyrolysis.[1,3,5] In this study, V_2O_5 thin-film nanostructures were prepared by spray pyrolysis using high-purity V_2O_5 powder dissolved in distilled water as precursor. The nanoparticle films were characterized by x-ray diffraction (XRD) analysis and field-emission scanning electron microscopy (FESEM). The sensing performance and efficiency of the resulting gas sensor based on V_2O_5 thin film are presented. This work focuses on light-enhanced gas sensors, i.e., activated by a green laser light source. To characterize the sensor performance towards ethanol and acetone vapors without and with light illumination, certain parameters were considered, viz. operation temperature, sensitivity, and response and recovery times. In view of this, the variation in the output current of the V_2O_5-based sensor when exposed to vapors of ethanol and acetone gases under different operating temperatures in the dark and under illumination was investigated to achieve the maximum response to the gas of interest.

EXPERIMENTAL PROCEDURES

Synthesis and Characterization of V_2O_5 Thin Films

V_2O_5 nanostructures with thickness of 423 nm were synthesized on glass substrates using pure V_2O_5 powder (purity 99.99%) by a spray technique, as described in a previous report.[24] Before the synthesis, substrates were cleaned with normal detergent, ethanol, and deionized distilled water. The spraying nozzle was positioned 28 cm away from the substrate. The spray flow rate was maintained at 4 ml/min using compressed nitrogen and pressure of 2 bar. The spraying solution contained V_2O_5 powder dissolved in deionized water at concentration of 0.1 M. Thin films of brown to yellow color were obtained at substrate temperature of T_s = 350°C.[25]

The structural properties of the prepared thin films were studied using x-ray diffraction (XRD) analysis (X'Pert PRD model, PANalytical Company), while their surface morphology was characterized by field-emission scanning electron microscopy (FESEM, MIRA3 model, TESCAN).

Gas Sensor Construction and Measurements

p-Type Si (100) was used as substrate for fabrication of the sensor device. Atmospheric-pressure chemical vapor deposition (APCVD) was used for growth of a 46.7-nm SiO_2 layer on the Si substrate. The APCVD system comprises a quartz reactor with diameter of 87 mm equipped with different accessories such as heating systems and control systems for the gas supply tubes. The surface of the silicon substrate was cleaned using the standard Radio Corporation of America (RCA) method, then dried by blowing air and placed at the center of a horizontal tube furnace.[26] The tube was heated to 900°C under wet O_2 gas at ambient pressure for 1 h to enable growth of SiO_2 on the Si surface. Afterwards, V_2O_5 nanostructures were deposited on SiO_2/Si using the spray pyrolysis technique, forming a *p*-type/insulator/*n*-type (PIN) structure. Metal contact areas (front and back) to the sensor were

formed by depositing high-purity metals onto the device surfaces via thermal evaporation under high-vacuum pressure of 10^{-5} mbar using an Edwards E-306 coating system. A mask consisting of an inter-digitated electrode with a 12-finger array was designed for the front Al contact, while Au was deposited on the entire back-side area to form the back contact.[25] The final configuration of the V_2O_5/SiO_2/Si sensor is illustrated in Fig. 1, where the output FESEM image was examined by Scanning Probe Image Processor (SPIP) software to probe the thickness of the V_2O_5 and SiO_2 layers.

To study the gas sensitivity of the sensor based on the prepared V_2O_5 nanostructures, an experimental setup was improvised as illustrated in Fig. 2. The setup consisted of the main experimental measurements performed on the sensor with two subparts labeled (a) and (b) for the sensor output measurements, as shown in Fig. 2.

The major components of the setup included a vacuum chamber (0.023 m^3 volume) covered by a cylindrical glass that allows light transmission to illuminate the sample, a vacuum pump for expelling air molecules from the chamber for replacement by vapor of the tested gas (ethanol or acetone) via two valves, a gas bottle source containing a liquid (ethanol or acetone) placed on a hot plate heater to obtain gas vapor, and a light illumination source (green laser light source) mounted 68 cm above the sample with fixed power of 200 mW/m^2 with its beam expanded uniformly to the sensor. The laser beam was chopped at 362 Hz by a fan to provide an on/off light reference. The sensor was kept within the chamber and heated by means of a small heater with a direct-current (DC) power supply and controlled by a calibrated K-type thermocouple. A double DC power supply was used to control the fan chopping frequency as well as the sensor temperature.

Electrical connections consisting of two copper wire probes with very low resistance were taken from the surface and back of the sensor to outside the chamber. The base of the chamber had two ports: one ending with a tube connected to the vacuum system and gas carrier bottles through two valves, and another used for electrical connection wires (electric leads, thermocouple, and heater wires) inside the chamber.[25] The output current of the sensor (connected through these wires) when exposed to gases under varying conditions was investigated by connecting the base chamber port to one of the two subparts (a) or (b), as illustrated in Fig. 2. Sensitivity measurements of the sensor were carried out as follows:

1. Connection to subpart (a)

This part was employed for current–voltage (I–V) measurements, where the device was connected directly to a picometer voltage source (Keithley 6487). The operation began with I–V measurements in the dark and at room temperature, with the light source and fan turned off. The I–V measurements were carried out when the device was exposed to vapors of ethanol and acetone gases. The air molecules were replaced by gas vapor through reversible opening/closing of the vacuum/gas (V_2/V_1) valves using the vacuum pump. The I–V measurements were then repeated, with the light source (illumination) switched on, but the fan remaining off. The device was exposed to vapors of ethanol and acetone gas for 5 min at flow rate of 0.8 L/min for both cases, viz. in the dark and under illumination.

To determine the optimum operating temperature for the device under dark conditions with and without exposure to the two gases, the light source was turned off while the heater under the device was turned on. The output current in the dark with no illumination was measured against temperature for three bias voltages (1 V, 3 V, and 5 V) when the device was exposed to the vapors of ethanol and acetone for duration of 5 min at flow rate of 0.8 L/min.

2. Connection to subpart (b)

This section presents the response and recovery time measurements, using the sampling circuit and

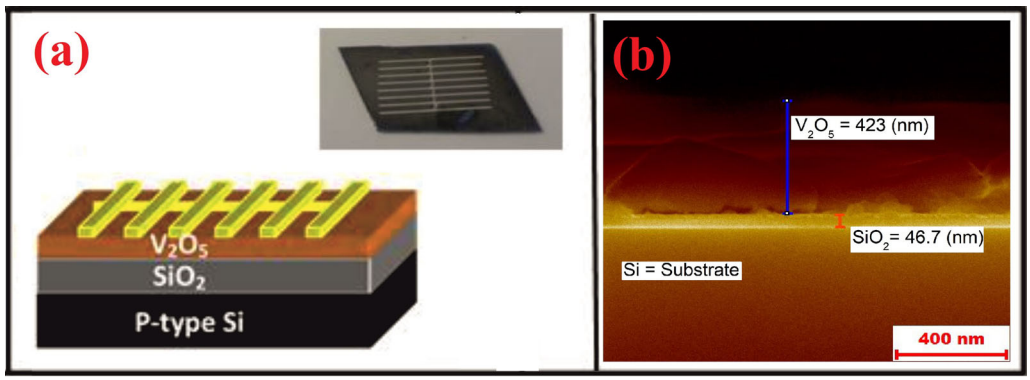

Fig. 1. (a) Schematic diagram with photographic image of the V_2O_5/SiO_2/Si sensor device in the chamber, and (b) cross-section image obtained by FESEM showing the thickness of the V_2O_5 and SiO_2 layers.

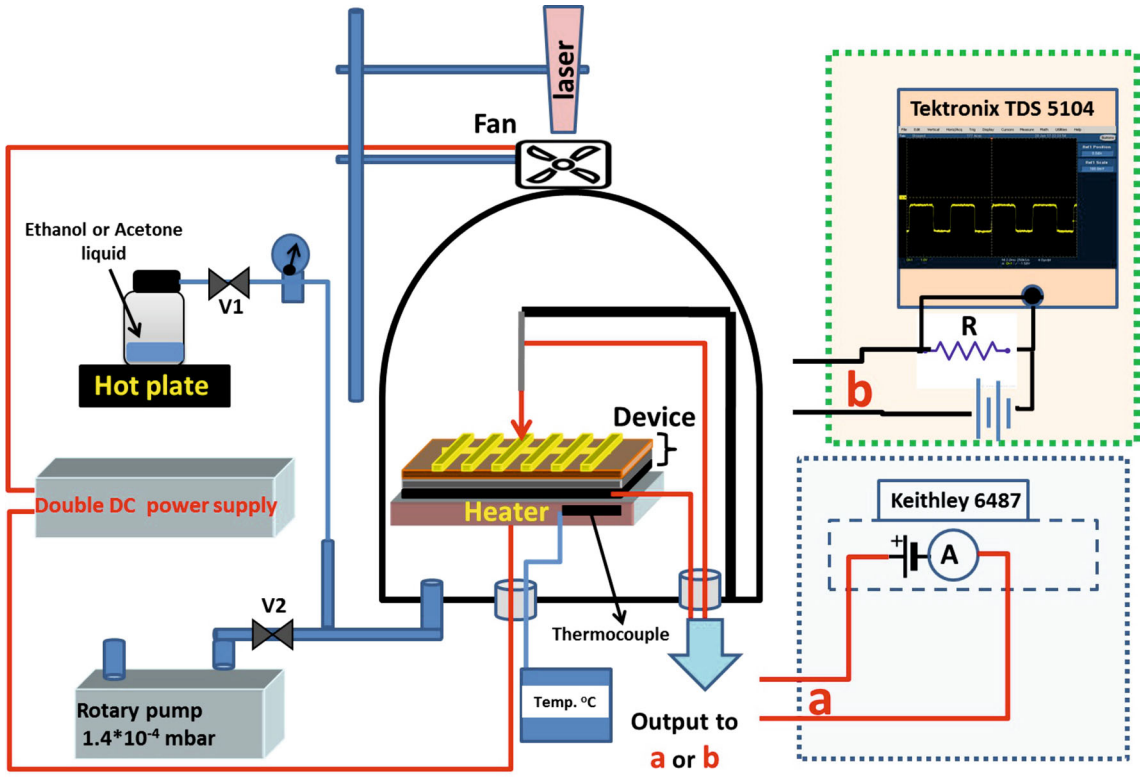

Fig. 2. Experimental setup for gas sensor measurements.

a high-resolution oscilloscope. The sampling circuit comprised the sample, a resistance coupled in series with the sample, and a DC power supply. The voltage of the sampling resistor, which reflects the variation in the photocurrent of the detector, was continuously recorded by a computerized oscilloscope (Tektronix TDS 5104) via acquisition of the value of the resistance (R) connected in series with the sample and the current passing through the resistor as well as the sample. The signals were then converted to obtain the sensitivity parameters of the sensor, as shown by subpart (b) in Fig. 2.

For this case, the light source and fan were turned on, and the variation in the output current signal versus time (I–t) at DC reverse bias of − 10 V was measured at room temperature under illumination without and with the gas vapors (ethanol and acetone). The device was exposed to the vapors for different durations (5 min, 10 min, and 15 min) at constant flow rate of 0.8 L/min to obtain different concentrations of each exposed gas.

RESULTS AND DISCUSSION

Structural and Morphological Characterization of V_2O_5 Thin Films

The XRD spectrum of V_2O_5 nanostructures synthesized at 350°C is depicted in Fig. 3. The peaks discernible in the spectrum denote the orthorhombic V_2O_5 phase structure with preferred orientation along (001) lattice plane at $2\theta = 20.264°$, with other weak signals from (301), (310), (002), (020), and (321) orientations at 30.308°, 35.265°, 41.150°, 50.603°, and 60.160°, respectively. All peaks are consistent with the values in standard Joint Committee on Powder Diffraction Standards (JCPDS) card no. 41-1426. The obtained results for orthorhombic V_2O_5 phase are in conformity with previous studies on V_2O_5 nanostructures.[27,28] The average crystallite size of the films was determined to be approximately 27.179 nm using the recognized Scherrer's formula.[8]

An FESEM image of the deposited V_2O_5 nanostructures is shown inset in Fig. 3. The V_2O_5 nanostructures consisted of well-defined large grains. The nanoparticles were agglomerated with near-spherical shape, being uniformly distributed on the surface of the substrate without any defects (pinholes or cracks). The small nanoparticles were susceptible to agglomeration, thereby forming larger nanoparticles that covered the substrate. This larger surface area improves the reaction between the V_2O_5 nanostructures and the exposed gas molecules as well as the interaction between the incident light and the film surface, which is important for gas sensing.[29] Based on the FESEM image, the average grain size was estimated to be approximately 62.3 nm.

Sensing Performance

Current–Voltage Characterization of the Sensor

The *I–V* characteristics of the fabricated V_2O_5 sensor structure were measured at room temperature in the range of − 8 V to 8 V; the results are shown in Fig. 4, where the effects of ethanol, acetone, and light illumination were investigated.

As observed, the *I–V* properties of the sensor measured in the dark with and without gas, and illuminated with gas, displayed diode-like exponential conductivity, indicating creation of a junction.[3] The forward current fluctuated exponentially with positive (+) applied bias voltage. In the case where the sensor was forward biased, flow of large current across the junction was enabled, as shown in Fig. 4. For reverse bias, only a small current could flow, since the reverse bias heightens the barrier. The small current generated by the reverse bias can largely be attributed to minority charge carriers from oxygen vacancies and/or impurities.

Use of the SiO_2 layer results in confinement, which helps development of an efficient device based on the $V_2O_5/SiO_2/Si$ structure. The presence of the SiO_2 layer might block transport of electrons from the V_2O_5 to Si, because the difference in the energy band offsets in the presence of the SiO_2 layer is slightly higher than that without the SiO_2 layer. The thinner interlayer oxide permits conduction of carriers by direct tunneling when a high voltage is applied on the device, so we already have current passing through the device, as for any other normal PIN device.[30] The ability of current to pass through

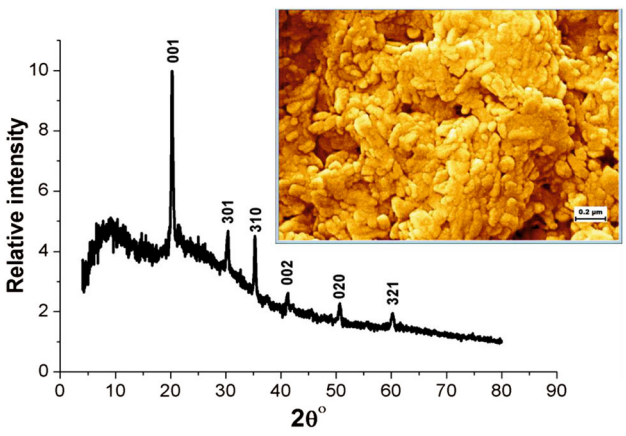

Fig. 3. XRD spectrum of V_2O_5 thin film synthesized on glass substrate via spray pyrolysis at 350°C. Inset shows FESEM image of V_2O_5 nanostructures (scale bar 0.2 μm).

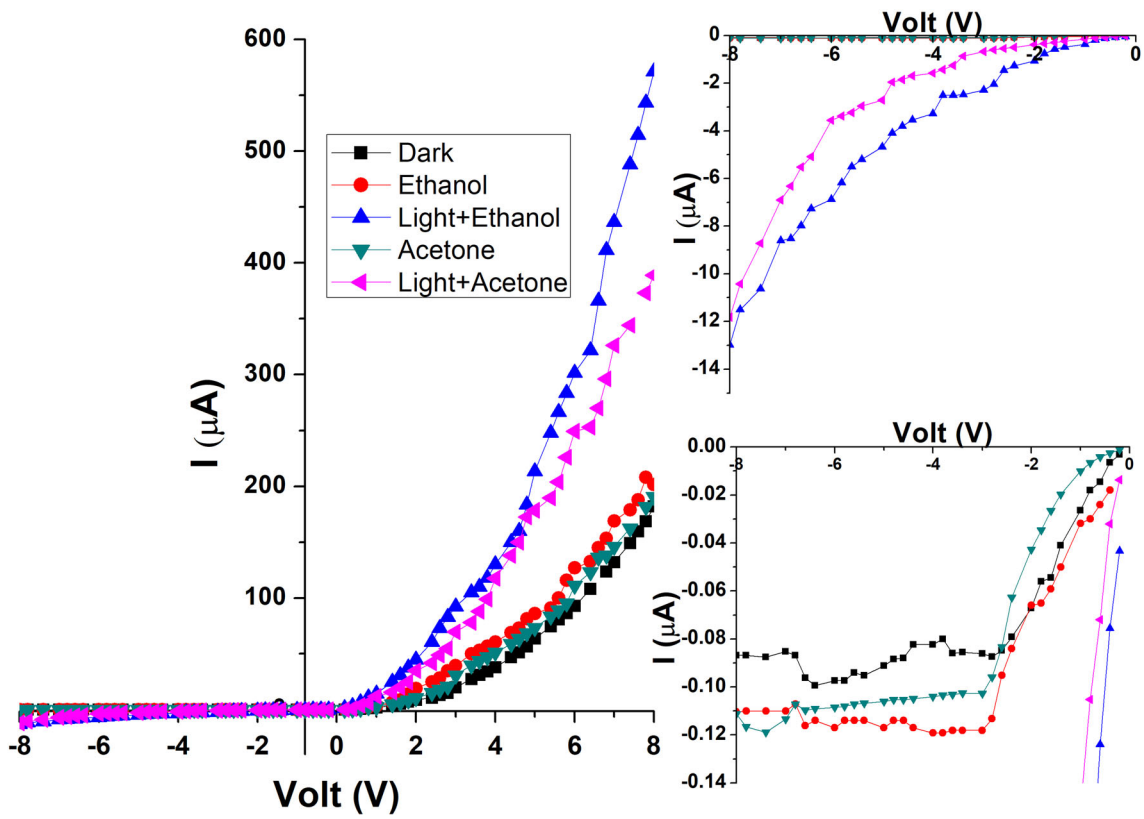

Fig. 4. *I–V* curves of $V_2O_5/SiO_2/Si$ sensor measured at room temperature under various conditions (i.e., dark with no gas, dark with gas, and gas with illumination). Insets shows the *I–V* relations at reverse bias in two low current ranges to illustrate the gas effect with (top) and without illumination (bottom).

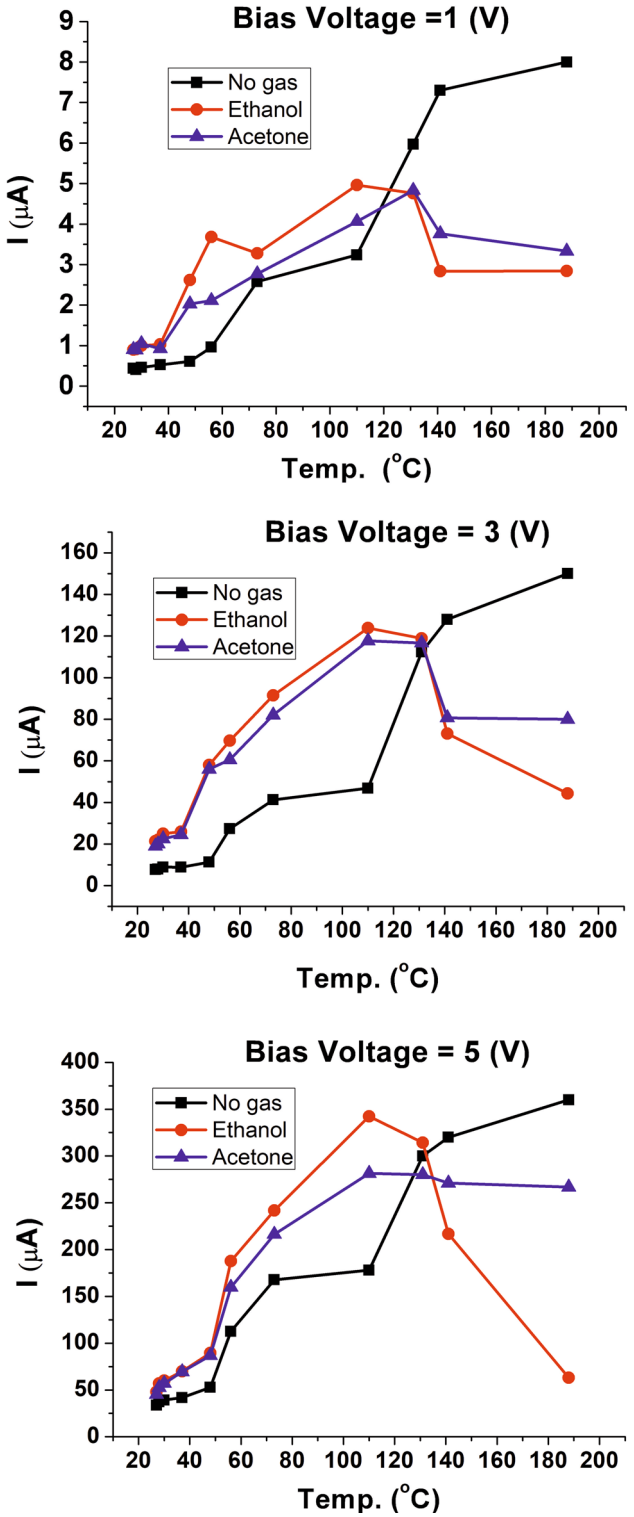

Fig. 5. Variation of current versus operating temperature for the $V_2O_5/SiO_2/Si$ sensor measured without and with gas (ethanol and acetone vapors) at three bias voltages.

the thin insulator and the effect of the gas on the number of charge carriers on the surface mean that the device will respond like any other gas sensor.

It is discernible from the *I–V* curves that exposure of the sensor to ethanol and acetone gases increased the current more under illumination compared with the dark current at similar bias voltages. This is because of the chemical interaction between adsorbed oxygen and the exposed gas, whereby the oxygen species reinserts the electron and increases the current. The current increased considerably when the sensor was exposed to the gases under illumination due to the increase in free charge carriers in the form of electron–hole pairs generated by the light illumination, as shown in the inset to Fig. 4. The role of illumination includes generation of electrons, which can be shifted into the conduction band, and holes that can recombine with electrons formerly trapped by the chemisorbed acceptor species, thus activating the desorption of molecules. In addition, the light provides activation energy needed for chemical reactions.[23] Hence, combining exposure to gas vapor with light illumination enhances the increase in conducting current of the sensor. Accordingly, the type of semiconductor will determine the behavior of the current variation or disparity. Therefore, for an *n*-type semiconductor, the released or free electrons lead to resistance reduction.[31]

It is important to consider the reverse-bias *I–V* characteristics shown inset in Fig. 4. Under reverse bias, the barrier height is so high that no current can traverse the device except for the extremely small thermal (saturated) current, where the function of SiO_2 as an insulator is to impede the current with increase in the applied voltage to a value lower than the collapse voltage, which indicates the device time off, causing the noise in the device to decrease. When the device is exposed to gas or gas under illumination, the current across the device begins to increase rapidly due to generation of relatively more carriers compared with the cases of no gas and in the dark, producing approximate straight-line downward curves, as clearly observed in the insets of Fig. 4, indicating the device time on. It was recently discovered that this on/off process is very good for several optoelectronic applications.[2,6,31]

Operating Temperature of the Sensor

The response of sensors based on metal-oxide semiconductors is influenced by their operating temperature. The adsorption of gases is dependent on the operating surface temperature of the sensing layer. To determine this temperature, the sensing response of the sensor was explored as a function of operating temperature. To achieve this objective, the current was measured with increase in operating temperature at three bias voltages (1 V, 3 V, and 5 V) with and without exposure to ethanol and acetone gases, as shown in Fig. 5.

It was found that exposure of the sensor to the gases initiated an increase in current, which was concomitant with increase in temperature because

Table I. Relative sensitivity of the $V_2O_5/SiO_2/Si$ sensor at different operating temperatures towards ethanol and acetone vapors in the dark and with illumination for different bias voltages, compared with results from literature with various configurations

Configuration	Operating temperature (°C)	Bias voltage (V)	Sensitivity in the dark (%) Eq. 1		Sensitivity with illumination (%) Eq. 2		Reference
			Ethanol	Acetone	Ethanol	Acetone	
Al/V_2O_5/SiO_2/Si/Au	Room temperature	1	68.34	27.63	623.61	253.73	This work (Fig. 4)
		3	97.00	54.10	361.25	76.82	
		5	35.17	15.37	235.58	107.55	
	48	1	330.34	233.05			This work (Fig. 5)
		3	412.36	394.369			
		5	69.95	64.51			
	110	1	53.08	25.51			
		3	164.40	151.10			
		5	92.25	58.05			
	188	1	− 64.5	− 58.33			
		3	− 70.46	− 46.66			
		5	− 82.5	− 25.92			
V_2O_5 spray pyrolysis	300–500		100–250				Ref. 16
V_2O_5-SnO_2 nanowire	60		283%				Ref. 6
V_2O_5 nanowire	330		90%				Ref. 35
V_2O_5 thin film	325		(10–125)%				Ref. 36

of the chemical reaction between the gas vapor and O_2 molecules adsorbed onto the sensor surface.[31] The maximum current value was observed in the intermediate temperature range. The current from the sensor was observed to decline slowly as the temperature was increased. The sensor response depends on the speed of the chemical reaction on the surface of the grains, and the speed at which gas molecules diffuse to that surface.[32] The minor sensor response at low temperatures is attributable to weak chemical activation between adsorbed gas molecules and the film surface due to the low thermal energy of the target that slows the reaction process. In the case of very high operating temperatures, the absorbed gas molecules may escape before reactions occur. Thus, the sensor response is constrained by the speed at which gas molecules diffuse to the surface, which is due to the complexities of the exothermic reaction at high temperature and the increased desorption rate of adsorbed molecules from the surface of grains, resulting in a weak sensor response.[31,32] At intermediate temperatures, the speed of the diffusion and desorption processes become equal, enabling the sensor response to attain its maximum value. For each gas, there is a specific temperature at which the sensor response reaches its maximum value.[33] In summary, the operating temperature is related to the reaction and activation energies between the adsorbed gas molecules and the sensing layer, which are influenced by the morphology and energy structure of the sensing material.

Sensitivity of the Sensor

The gas sensitivity (S) of a sensor is described as the ratio between the change in the output current from the sensor when exposed to a gas or a gas with illumination and the current at dark without exposure to gas to the current at dark without exposure to gas. The sensor sensitivity can be calculated for these two scenarios, i.e., exposure to gas (S_g) and exposure to gas with illumination (S_{g+I}), using Eqs. 1 and 2, respectively[12,34]:

$$S_g = \frac{I_g - I_d}{I_d}, \quad (1)$$

$$S_{g+I} = \frac{I_{g+I} - I_d}{I_d}, \quad (2)$$

where I_d, I_g, and I_{g+I} are the current measured in the dark with no gas, with gas vapor, and with both gas vapor and illumination, respectively.

Using Eqs. 1 and 2, the relative sensitivity of the sensor was determined at different operating temperatures without illumination (in the dark) and with illumination, when exposed to ethanol and acetone gases, at three forward bias voltages (1 V, 3 V, and 5 V), as shown in Figs. 4 and 5. The obtained results are summarized in Table I along with the sensitivities of different V_2O_5-based gas sensors reported in literature.[6,16,35,36]

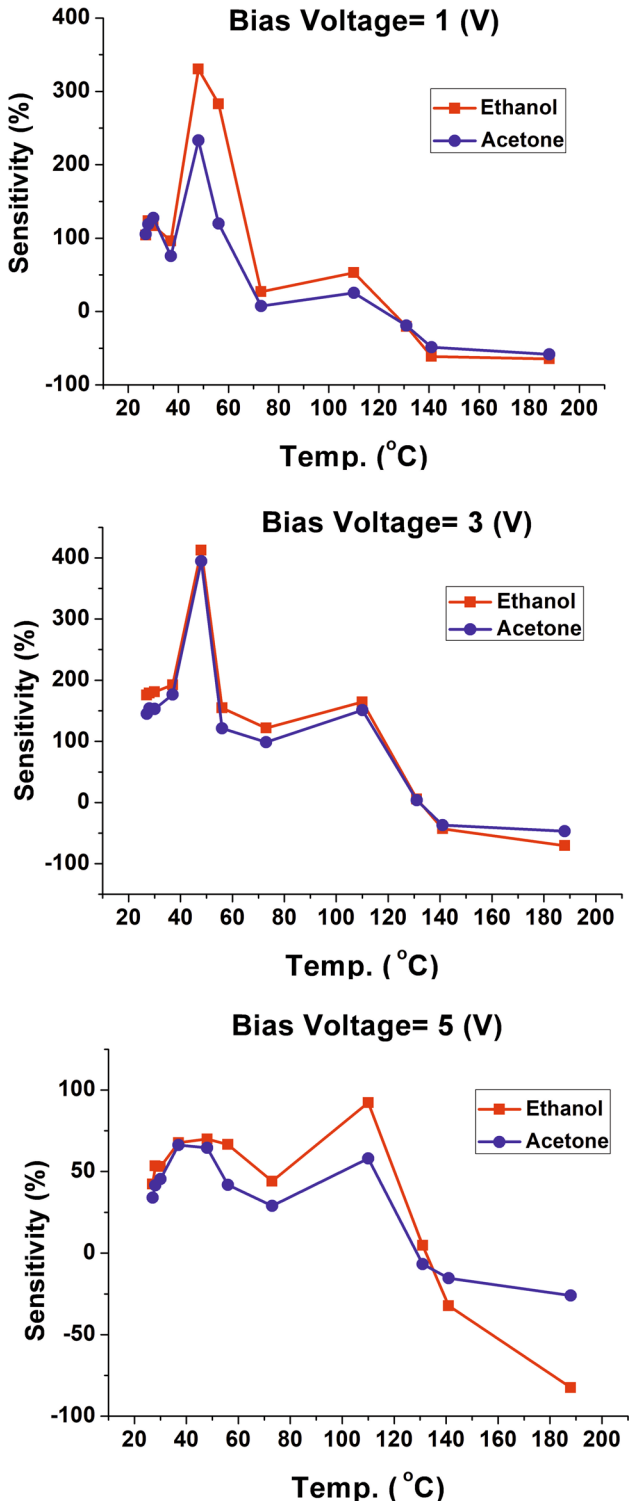

Fig. 6. Relative sensitivity versus operating temperature of the $V_2O_5/SiO_2/Si$ sensor measured in the dark with no gas and towards ethanol and acetone vapors at three bias voltages.

It can be inferred that light illumination could improve the sensitivity of the film. The sensor

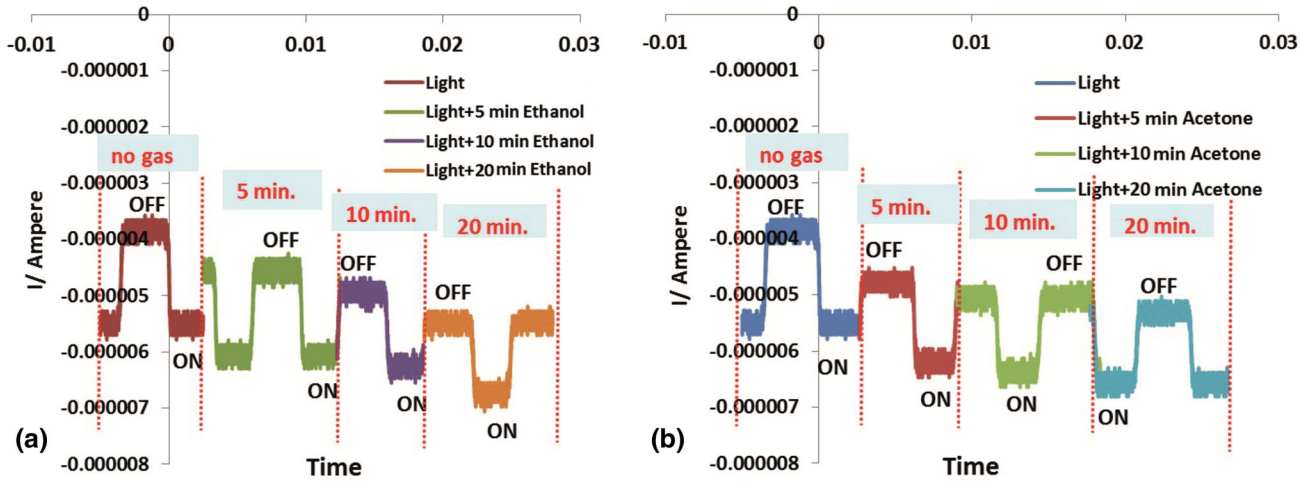

Fig. 7. Repeatability dynamic response (on/off) of the time-dependent photocurrent signal from the $V_2O_5/SiO_2/Si$ sensor at DC bias of − 10 V when illuminated with light (on/off) with no gas and when exposed to gas vapor for different times (5 min, 10 min, and 20 min) for ethanol (a) and acetone (b).

sensitivity when exposed to ethanol gas was slightly higher than for acetone, with and without illumination. At bias voltage of 1 V, the relative sensitivity of the sensor increased to 68.34% when exposed to ethanol in the dark and to 623.61% when exposed to ethanol and illuminated. The relative sensitivity increased to 27.63% when exposed to acetone and to 253.73% when exposed to acetone and illuminated, as shown in Table I. These sensitivity results indicate that illumination enhanced the generation efficiency of carriers. The net concentration of carriers with illumination was relatively higher than those generated with only the gas reaction, confirming the higher generation of free carriers and oxygen ionosorption under illumination. In general, the results show two competing contributions from light irradiation, i.e., increased electron–hole pair concentration and increased oxygen ionosorption.[12,32]

The effect of the operating temperature on the sensitivity of the sensor was also determined based on the aforementioned results (Fig. 5) and Eq. 1. The relative sensitivity versus operating temperature of the $V_2O_5/SiO_2/Si$ sensor measured in the dark with no gas and when exposed to ethanol and acetone vapor at three bias voltages is shown in Fig. 6.

Higher sensor sensitivity values were observed at lower operating temperatures. The optimum operating temperature range was determined to be 40°C to 50°C. When the optimum temperature was exceeded, the sensitivity of the sensor was observed to decrease gradually until becoming negative at temperatures > 110°C. These operating temperatures are lower compared with others reported in previous studies.[2,31] All the obtained results (Table I and Fig. 6) show that the $V_2O_5/SiO_2/Si$ sensor exhibited higher sensitivity towards ethanol than acetone, possibly due to faster evacuation of charge carriers when exposed to ethanol.

Furthermore, the sensing characteristics of the sensor as a function of time were investigated under dark conditions and when exposed to light illumination without and with gas (ethanol and acetone) at different times (5 min, 10 min, and 20 min) and bias DC voltage of − 10 V. The output current signal as a function of time for these conditions is shown in Fig. 7.

The output current–time signals in Fig. 7 were used to determine the response and recovery times of the sensor (Fig. 8) at room temperature for each condition, as summarized in the table in the figure.

From the results in Fig. 8, it can be deduced that the sensor response increased with increase in the duration of exposure to both ethanol and acetone vapors. The best response and recovery times were obtained at exposure duration of 10 min. The response and recovery times were determined to be 43.493 μs and 195.42 μs for ethanol, and 43.2001 μs and 214.17 μs for acetone, respectively. Furthermore, it was also observed that the response and recovery times increased with increase in the duration of exposure to gas, possibly due to the low vapor and diffusion rate resulting from the saturation effect as well as the increasing pressure inside the chamber as the gas concentration increased. The response and recovery times indicate that the sensor exhibited significant sensing properties towards ethanol and acetone at low temperature, supporting the applicability of this sensing device.

SENSING MECHANISMS

PIN Diode Mechanisms

Generally, a PIN diode is a semiconductor device that consists of an insulator or intrinsic (i) region sandwiched between a *p*-type and *n*-type layer. A

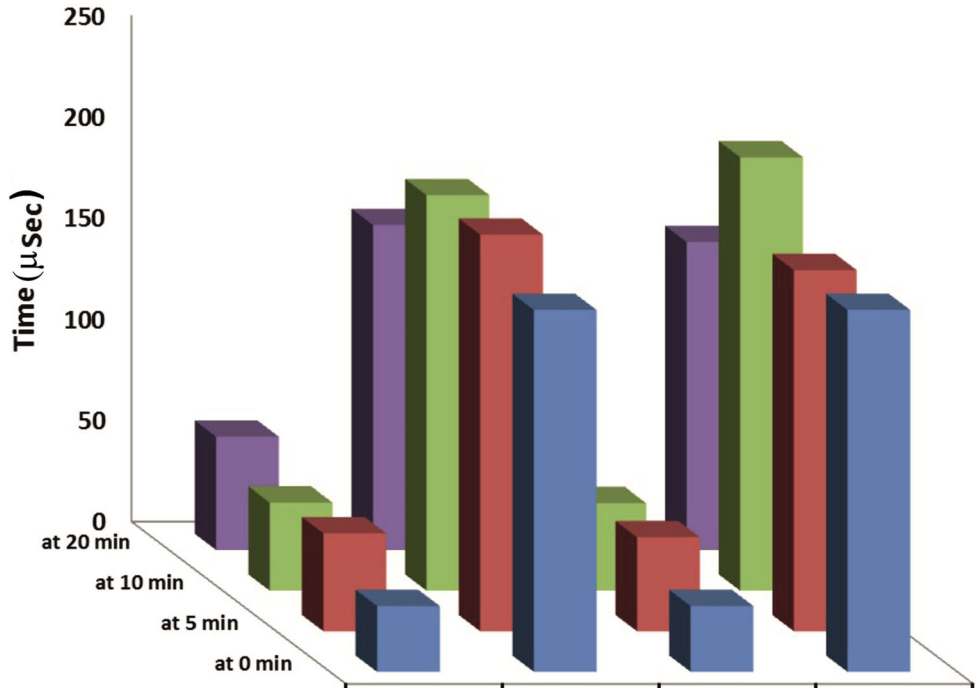

	Response time (Ethanol) μsec	Recovery time (Ethanol) μsec	Response time (Acetone) μsec	Recovery time (Acetone) μsec
at 0 min	32.531	178.8	32.531	178.8
at 5 min	48.44	195.95	46.47	178.47
at 10 min	43.493	195.42	43.2001	214.17
at 20 min	55.869	160.62	53.818	152.2

Fig. 8. Response and recovery times versus gas exposure time for the sensor, as summarized in the table.

PIN diode operates under what is known as higher-level injection. In other words, the intrinsic region is flooded with charge carriers from the *p*- and *n*-regions. Its function can be likened to filling up a water bucket with a hole on the side. Once the water reaches the level of the hole, it will begin to pour out. Similarly, the diode will conduct current once it reaches an equilibrium point at which the number of electrons is equal to the number of holes in the intrinsic region.

When the diode is forward biased, the injected carrier concentration is typically several orders of magnitude higher than the intrinsic carrier concentration. Due to this higher-level injection, which in turn is due to the depletion process, the electric field extends deeply into (over almost the entire length of) the region. This electric field helps speed up transport of the charge carriers from the *p* to *n* region, resulting in faster operation of the diode, making it a suitable device for high-frequency operation. The frequency at which a PIN diode stops to act like a PN diode and starts acting like a linear variable resistor is called the transition frequency. The transition frequency is a function of the thickness of the intrinsic layer. When the PIN diode is reversed biased, the reverse voltage will keep on increasing the width of the depletion region at the N–I junction. It will increase up to the point at which the entire intrinsic layer is swept or free from charge carriers. PIN diodes in reverse bias are used in various devices such as photodetectors and in high-voltage electronics applications.

The sensitivity of a photodetector is normally defined by the ratio of the photocurrent to the power of the incident radiation. A photodiode working in reverse bias exhibits constant photocurrent with the reverse voltage, as long as it does not enter the breakdown region. The dark current is equal to the reverse saturation current, which may increase with the reverse voltage. In the case of a PIN photodetector, the high voltage present in the depletion region causes photogenerated carriers to separate and be collected across the reverse-biased junction. This gives rise to a current flow known as the photocurrent. The photocurrent may increase linearly with the applied voltage, while the dark current may increase linearly at low voltage, then more than linearly at higher voltage, because of

heating effects. Therefore, the ratio will be constant at low voltage when the heating effect is negligible but decrease at high voltage because of such heating effects. One can prove this by measuring the current as a function of voltage.[37]

Metal Oxide and Light-Enhanced Metal Oxide Gas Sensor Mechanisms

In general, the sensing mechanism of metal-oxide gas sensors is based on exchange of electrons between adsorbed gas species and the metal oxide. Transition-metal oxides such as V_2O_5 are known metal oxide materials for manufacture of gas sensors.[2,22,38] Previous studies reported that the conductivity of a gas sensor is changed by the chemisorption of oxygen species on the sensor's surface.[39–44] These studies explained that, when a metal-oxide sensor is exposed to air, adsorption of O_2 molecules on the surface leads to electron transfer from the conduction band of the metal oxide to oxygen molecules, resulting in formation of O_2^- and O^- ions and inducing a space-charge region at the surface, which serves as a potential barrier for electron conduction, consequently increasing the surface resistivity. Therefore, exposure of the metal-oxide surface to air results in lower conductivity.[42] When the sensor surface is exposed to a gas (such as ethanol or acetone), the gas reacts with adsorbed oxygen, causing the oxygen species to reinject electrons, and increasing the metal oxide conductivity.[38] When the sensor is exposed again to air, oxygen from the atmosphere is adsorbed and bonds with electrons on the surface of the sensor, restoring the initial resistance value. This means that the sensor can be used as a switching (on/off) device with and without gas.[7]

The surface sensing mechanism of the V_2O_5 nanostructures towards ethanol or acetone with and without light illumination can thus be explained as follows:

When the V_2O_5 nanostructures are exposed to air, oxygen molecules from the air are adsorbed onto the surface, thereby trapping electrons to form adsorbed oxygen ions through the reaction expressed in Eq. 3.[33,39,40,44]

$$O_{2(ads)} + e^- = O_2^- \quad (3)$$

These oxygen ions are distributed on the surface of the V_2O_5 in the form of VO surface groups. The VO groups are located on the lowest free energy surface of V_2O_5 (001 plane), as confirmed by XRD analysis, to produce an electron depletion region with high electric potential.[39]

When V_2O_5 thin film is exposed to ethanol (C_2H_5OH) gas, the gas molecules react with adsorbed O_2^-, O^-, and O^{2-} ions on the surface of the V_2O_5 thin film. These reactions increase the concentration of electrons on the surface of V_2O_5, thus decreasing the resistance of the V_2O_5 layer. The interaction between ethanol gas and oxygen species is illustrated by Eqs. 4 to 7.[41]

$$O_2^- + C_2H_5OH_{(g)} \rightarrow H_2O_{(g)} + 2CO_{2(g)} + e^- \quad (4)$$

$$3O_2^- + C_2H_5OH_{(g)} \rightarrow 3H_2O_{(g)} + 2CO_{2(g)} + 3e^- \quad (5)$$

$$O_2^{2-} + C_2H_5OH_{(g)} \rightarrow H_2O_{(g)} + 2CO_{2(g)} + 2e^- \quad (6)$$

$$3O_2^{2-} + C_2H_5OH_{(g)} \rightarrow 3H_2O_{(g)} + 2CO_{2(g)} + 6e^- \quad (7)$$

A schematic of the surface sensing mechanism of the V_2O_5 nanostructures towards ethanol or acetone is shown in Fig. 9.

The mechanism for light-enhanced sensing by metal oxides relies on formation of photogenerated carriers in the gas adsorption/desorption process, which increases the density of charge carriers through generation of electron–hole pairs. The reactions between the generated electron–hole pairs and oxide species lead to weak bonding of oxygen species with the oxide surface.[22,29] When light illuminates the metal oxide, chemisorbed oxygen species are desorbed by interacting with photogenerated electrons. Afterward, the resistivity of the metal oxides decreases due to the reduction in the thickness of the space-charge layer. Upon exposure

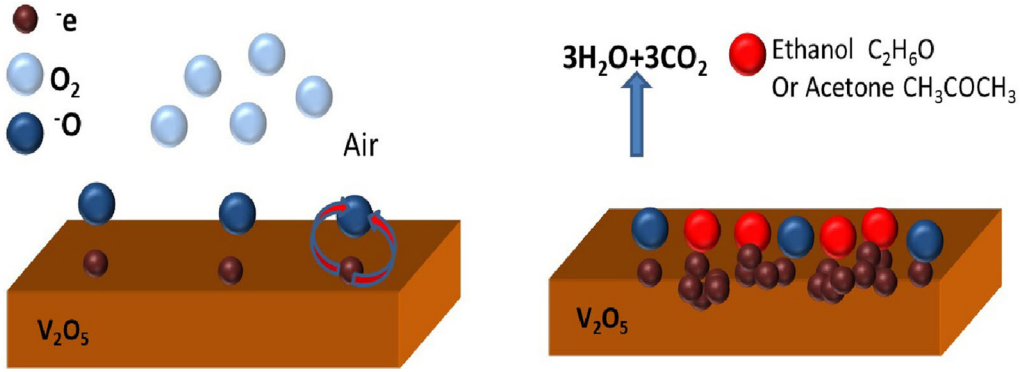

Fig. 9. Schematic of the surface sensing mechanism of V_2O_5 nanostructures towards ethanol or acetone.

to a target gas, photogenerated holes recombine with electrons from the target gas, causing electron–hole separation, which decreases the resistance across the metal oxide.[22] The *I–V* curves under light illumination (Fig. 4) show enhanced current conduction for the sensor, which in turn enhances the sensing performance when compared with the dark current, as observed in Table I.

It can be inferred from these results that $V_2O_5/SiO_2/Si$ is a promising candidate for use in high-performance commercial gas sensors that are effective at low temperatures. It can also be suggested that light illumination is a promising method for activating the sensitivity of such gas sensors at low temperature.

CONCLUSIONS

V_2O_5 thin films were deposited by spray pyrolysis technique. Structural and morphological characterization confirmed that the films were homogeneous and contained V_2O_5 phase with nanostructure grain size. A highly sensitive $V_2O_5/SiO_2/Si$ gas sensor was developed by depositing V_2O_5 nanostructures on oxidized *p*-type silicon substrate (SiO_2/Si). The gas response was significantly improved when illuminated with a green laser light source due to the increased density of free charge carriers. The sensitivity of the sensor towards ethanol and acetone was higher at low operating temperatures (40°C to 50°C). The $V_2O_5/SiO_2/Si$ gas sensor was more sensitive to ethanol than acetone at room temperature under both dark and illumination conditions. In addition, the sensor exhibited faster response/recovery time for ethanol (43.493 μs/195.42 μs) than acetone (43.2001 μs/214.17 μs) at exposure duration of 10 min. Therefore, application of such V_2O_5 nanostructures is promising for detection of both acetone and (particularly) ethanol at low operating temperatures.

REFERENCES

1. M.C. Rao, *Int. J. Chem. Tech. Res.* 6, 1904 (2014).
2. K. Schneider, M. Lubecka, and A. Czapla, *Sens. Actuators B Chem.* 236, 970 (2016).
3. C.M. Hung, D.T.T. Le, and N. Van Hieu, *J. Sci. Adv. Mater. Dev.* 2, 263 (2017).
4. A.R. Muchtar, N.L.W. Septiani, M. Iqbal, A. Nuruddin, and B. Yuliarto, *J. Electron. Mater.* (2018). https://doi.org/10.1007/s11664-018-6213-x.
5. N.C. Vieira, W. Avansi, A. Figueiredo, C. Ribeiro, V.R. Mastelaro, and F.E. Guimarães, *Nanoscale Res. Lett.* 7, 310 (2012).
6. R. Wang, S. Yang, R. Deng, W. Chen, Y. Liu, H. Zhang, and G.S. Zakharova, *RSC Adv.* 5, 41050 (2015).
7. A. Dhayal Raj, T. Pazhanivel, P. Suresh Kumar, D. Mangalaraj, D. Nataraj, and N. Ponpandian, *Curr. Appl. Phys.* 10, 531 (2010).
8. R.S. Ganesh, E. Durgadevi, M. Navaneethan, V.L. Patil, S. Ponnusamy, C. Muthamizhchelvan, S. Kawasaki, P.S. Patil, and Y. Hayakawa, *J. Alloys Compd.* 721, 182 (2017).
9. H.H. Güllü, Ö. Bayraktar, D.E. Yıldız, and M. Parlak, *J. Electron. Mater.* (2018). https://doi.org/10.1007/s11664-018-6155-3.
10. A.M. Soleimanpour, A.H. Jayatissa, and G. Sumanasekera, *Appl. Surf. Sci.* 276, 291 (2013).
11. M. Boshta, F.A. Mahmoud, and M.H. Sayed, *J. Ovonic Res.* 6, 93 (2010).
12. K. Govardhan and A.N. Grace, *J. Sens.* (2016). https://doi.org/10.1155/2016/7652450.
13. G.J. Shyju, S. Nagarani, S.D.D. Roy, and C. Sanjeeviraja, *Arch. Appl. Sci. Res.* 4, 2149 (2012).
14. X. Liu, S. Cheng, H. Liu, S. Hu, D. Zhang, and H. Ning (2012). https://doi.org/10.3390/s120709635.
15. S. Pandey, *J. Sci. Adv. Mater. Devices* 1, 431 (2016).
16. K. Schneider, M. Lubecka, and A. Czapla, *Sens. Actuators B* 236, 970 (2016).
17. I. Raible, M. Burghard, U. Schlecht, A. Yasuda, and T. Vossmeyer, *Sens. Actuators B* 106, 730 (2005).
18. A.S. Chizhov, M.N. Rumyantseva, R.B. Vasiliev, D.G. Filatova, K.A. Drozdov, I.V. Krylov, A.V. Marchevsky, O.M. Karakulina, A.M. Abakumov, and A.M. Gaskov, *Thin Solid Films* (2016). https://doi.org/10.1016/j.tsf.2016.09.029.
19. S.P. Chang and K.Y. Chen, *ISRN Nanotechnol.* (2012). https://doi.org/10.5402/2012/453517.
20. C. Zhang, A. Boudiba, C. Bittencourt, R. Snyders, M.G. Olivier, and M. Debliquy, *Procedia Eng.* 47, 116 (2012).
21. E. Comini, *Sensors* 13, 10659 (2013).
22. M. Cho and I. Park, *J. Sensor Sci. Technol.* 25, 103 (2016).
23. S.P. Ghosh, K.C. Das, N. Tripathy, G. Bose, D.H. Kim, T.I. Lee, J.M. Myoung, and J.P. Kar, *Mater. Sci. Eng.* 115, 012035 (2016).
24. T.A. Abbas, L.H. Slewa, H.A. Khizir, and Sh.A. Kakil, *J. Mater. Sci. Mater. Electron.* 28, 1951 (2017).
25. T.A. Abbas, L.H. Slewa, and Sh.A. Kakil, *J. Mater. Sci. Mater. Electron.* 28, 16086 (2017).
26. Y.M. Hassan and Sh.A. Kakil, *J. Mater. Sci. Mater. Electron.* 26, 6092 (2015).
27. Z. Li, J. Cai, P. Cizek, H. Niu, Y. Du, and T. Lin, *J. Mater. Chem. A* 3, 16162 (2015).
28. N.M. Abd-Alghafour, N.M. Ahmed, and Z. Hassan, *Sens. Actuators A* 250, 250 (2016).
29. X. Fang, Y. Bando, M. Liao, T. Zhai, U.K. Gautam, L. Li, Y. Koide, and D. Golberg, *Adv. Funct. Mater.* 20, 500 (2010).
30. L.G. Gerling, G. Masmitja, P. Ortega, C. Voz, and R. Alcublla, *Energy Procedia* 124, 584 (2017).
31. X.H. Yang, H. Xie, H.T. Fu, X.Z. An, X.C. Jiang, and A.B. Yu, *RSC Adv.* (2016). https://doi.org/10.1039/C6RA18848F.
32. A. Sanger, A. Kumar, A. Kumar, J. Jaiswal, and R. Chandra, *Sens. Actuators B* 236, 16 (2016).
33. R.H. Bari and S.B. Patil, *Int. Lett. Chem. Phys. Astron.* 17, 125 (2014).
34. M.L. Zeggar, F. Bourfaa, A. Adjimi, M.S. Aida, and N. Attaf, *Mater. Sci. Eng.* 108, 012004 (2016).
35. G. Micocci, A. Serra, A. Tepore, S. Capone, R. Rella, and P. Siciliano, *J. Vac. Sci. Technol. A* 15, 34 (1997).
36. A.D. Raj, P.S. Kumar, Q. Yang, and D. Mangalaraj, *Physica E* 44, 1490 (2012).
37. W. Ahmad, M.U. Alic, V. Laxmid, and A.S. Syed, *Asian J. Nanosci. Mater.* 1, 122 (2018).
38. R.K. Nath and S.S. Nath, *Sens. Mater.* 12, 59 (2009).
39. S.A. Hakim, Y. Liua, G.S. Zakharovab, and W. Chen, *RSC Adv.* 5, 23489 (2015).
40. M. Abbasi, S.M. Rozati, R. Irani, and S. Beke, *Mater. Sci. Semicond. Process.* 29, 132 (2015).
41. V. Kruefu, P. Pookmanee, A. Wisitsoraat, and S. Phanichphant, *Key Eng. Mater.* 659, 259 (2015).
42. M.S. Lemraski and E. Nadimi, *Surf. Sci.* 657, 96 (2017).
43. Y. Wang, Y. Zhou, C. Meng, Z. Gao, X. Cao, X. Li, L. Xu, W. Zhu, X. Peng, B. Zhang, and Y. Lin, *Nanotechnology* 27, 425503 (2016).
44. T.I. Nasutiona, I. Nainggolan, S.D. Hutagalung, K.R. Ahmad, and Z.A. Ahmad, *Sens. Actuators B* 177, 522 (2013).